JOURNAL OF MATERIALS SCIENCE 24 (1989) 3011–3020

Structure of oxide gels and glasses by infrared and Raman scattering

Part 2 *Mullites*

Ph. COLOMBAN
Laboratoire de Physique de la Matière Condensée-Chimie du Solide, UA 1254 – CNRS, Ecole Polytechnique, 91128 Palaiseau, and Laboratoire de Spectrochimie IR et Raman, CNRS, 2 rue H. Dunant, 94320 Thiais, France

Optically clear monolithic gels (and powders) have been synthesized using various silicon alkoxides and different hydrolysis conditions. Thermal treatments lead to optically clear (translucent if compacted powders are used) glasses and ceramics. The structure of the gel and its transformation in glass and in crystalline ceramic have been studied by X-ray, DTA, TGA, IR and Raman spectroscopies. Mullite gels show broad spectra similar to alumina gels, whereas germanium substitution leads to narrower bands located at lower frequencies according to the mass effect. The gel structure is of spinel-type. Use of alkoxides with long organic chains favours heterogeneities. Formation of the glass and also of the true spinel structure, does not modify the Raman spectra to any great extent whereas large modifications are observed on IR spectra with the evolution of protonic species. Continuous transformation of spinel into mullite spectra between 1000 and 1600° C, together with band narrowing, indicates a progressive evolution which explains the large nonstoichiometry range. In particular the narrowing of the SiO_4 stretching mode ($\nu = 970\,cm^{-1}$) seems to indicate a progressive ordering (history dependent) of the SiO_4 environment.

1. Introduction

The preparation of monolithic gels through sol–gel methods, leading by low-temperature anneals to glasses and ceramics, has attracted considerable attention in recent years [1–5]. The gel route offers specific advantages, for instance, a submicronic homogeneity, fine microstructure, and the sintering temperature as well as the crystallinity may be chosen [5, 6]. This last point is particularly interesting for nonstoichiometric compounds.

Mullite is an aluminosilicate refractory with composition $Al_2[Al_{2+2x}Si_{2-2x}]O_{10-x}$, with the composition variable x ranging (in principle) from 0 to 1. When $x = 0$, the structure is that of (disordered) sillimanite, Al_2SiO_5, while at $x = 1$ it resembles the structure proposed for the iota polymorph of alumina [7–13]. This range of composition is based upon the exchange $2Si^{4+} + O^{2-} \rightarrow 2Al^{3+}$ which requires the formation of oxygen vacancies. As shown in Fig. 1, the formation of one such vacancy in the sillimanite → mullite derivation leads to the rotation of one tetrahedron.

As indicated in Part 1 [14], only a few works have used the vibrational spectroscopy to understand the structure of such disordered materials. McMillan and Piriou [15] recorded Raman spectra of various mullites quenched from high temperatures after solar furnace melting and compared their spectra with those of the parent crystalline (sillimanite, andalousite and kyanite) and of parent glassy compounds. As shown in Fig. 1, sillimanite may be described as edge-shared ribbons of AlO_6 octahedra aligned in the c-direction, cross-linked by corner-shared AlO_4 and SiO_4 tetrahedra. Four aluminium atoms per unit-cell are in octahedral sites, while four are in tetrahedral sites. The low-temperature polymorph, andalousite, is also based on edge-shared AlO_6 ribbons, but cross-linked by irregular AlO_5 polyhedra and SiO_4 tetrahedra. There is one AlO_6 octahedron per five-fold coordinated aluminium in the structure. Finally, the most dense high-pressure phase kyanite, has a network of AlO_6 octahedra and SiO_4 tetrahedra [9, 11].

In fact, the mullite structure is not fully disordered and diffuse electron scattering indicates local ordering [8, 12, 16]. Recent work of Angel and Prewitt [10] interprets the diffusion with the presence of two ordering schemes, both of which resemble ordering patterns found in the related stoichiometric structures, sillimanite and i-alumina, these two ordering patterns fit together in such a way as to allow the incommensurate mullite structure to employ both ordering schemes simultaneously.

The formation of mullite through various methods (solid state reactions from kaolin or from ball-milled amorphous or crystalline oxides, sol–gel routes, etc) have been extensively studied (see, for instance, [17–30]). Recently Okada and Otsuka [31] have given a good survey of the question. However, the structure of the mullite gel and glass as well as the nature of the phase(s) occurring before the formation of the orthorhombic mullite framework remains open to question.

0022–2461/89 $03.00 + .12

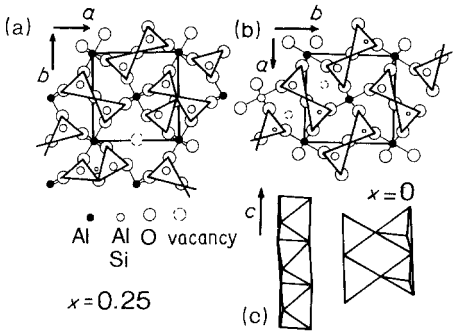

Figure 1 Schematic drawing of the mullite ($Al_{4+2x}Si_{2-2x}O_{10-x}$) structure evolution as a function of x: (a) mullite unit cell ($x = 0.25$) projected on the a, b plane. An oxygen vacancy is indicated by a broken circle [8]; (b) partial projection of the sillimanite structure ($x = 0$) in the a, b plane; broken circles (squares) and arrows show the hypothesized shifts of aluminium atoms for sillimanite–andalousite (kyanite) conversion [13]; (c) polyhedral AlO_6 chains parallel to the c-axis for sillimanite.

The major controversy concerns the intermediate phase occurring before the orthorhombic mullite phase. Using kaolin as raw material, metakaolinite is formed at $\simeq 600°$ C and a cubic phase is formed at 980° C; orthorhombic mullite is formed at the second exotherm (1250° C). Chakraborty and Ghosh [19] concluded that the cubic phase has the composition $3Al_2O_3 \cdot 2SiO_2$ and that the excess silica was liberated at the first exotherm. Other work [20, 26] suspected a segregation of γ-alumina (having the spinel structure) and silica before mullite formation. In the case of sol–gel methods [7, 22, 25, 29, 30] the situation differs as a function of the "gel homogeneity". Heterogeneities induce the formation of crystobalite and/or corundum. On the other hand, homogeneous gels exhibit differential thermal analysis (DTA) peaks at 980 and 1250° C with formation of mullite at the first exotherm. Optically clear mullite ceramics have been obtained after high-temperature sintering for compositions near 63% Al_2O_3 [25, 30]. Okada and Otsuka [31] summarize four typical cases for kaolin evolution above 980° C.

Heterogeneous mixing

Amorphous silica + γ-alumina $\xrightarrow{1350°C}$ mullite (+ crystobalite)
Amorphous silica + γ-alumina $\xrightarrow{1000°C}$ corundum

Homogeneous gel

Spinel ($6Al_2O_3$–SiO_2) + am. silica with 8% Al $\xrightarrow{1150°C}$ mullite $\xrightarrow{1350°C}$ (crystobalite)

Metakaolinite

Non-stoichiometric mullite + spinel (6/1) amorphous silica $\xrightarrow{1150°C}$ mullite $\xrightarrow{1400°C}$ (crystobalite)

Glass

$\xrightarrow{980°C}$ mullite

From the micronic scale heterogeneous mixing of oxide powders to the "molecular mixing" achieved in glass the size of local inhomogeneities decreases and thus the temperature needed for mullite formation also decreases.

In this paper, we try to understand the local structure of mullite gels and glasses and the influence of synthesis on this structure. Preliminary results have been published [32].

2. Experimental procedure

2.1. Synthesis

Two routes have been used: the slow (monolith synthesis) and the rapid (powder synthesis) hydrolysis route as in the case of many other materials [5, 6].

2.1.1. Slow route

A propanol, hexane or cyclohexane solution of aluminium sec-butoxide (Alfa-Ventron, Karlsruhe) and silicon alkoxides (methoxide, ethoxide, sec-butoxide, i-propoxide; Alfa-Ventron, Karlsruhe and Dynamit-Nobel, Chemirolo, Tzuisdorf) was slowly hydrolysed with atmospheric moisture ($\sim$ relative humidity 60%). First the aluminium sec-butoxide was diluted in propanol (volume ratio 1/4). Two kinds of solvent were used: alcohols (for instance propanol) and hexane (or cyclohexane). These last solvents are non-protic and non-polar media. The solutions were kept in a Petri Box (diameter 100 mm, height 10 mm) or in a covered bottle (diameter $\sim$ 30 mm, height 100 mm). The water vapour meets the solution surface through gas invasion at the interstices between the box (bottle) and the cover or through small pin-holes in the cover. The respective solvent/alkoxide ratios are given in Table I. After weeks or months, monolithic optically clear gels were obtained and were dried between 30 and 60° C, for 1 week. Drying induced cracks and the size of the monolithic pieces was reduced to about 0.1 to 1 cm^3. For comparison, monoliths were also prepared using $Al(NO_3)_3$ aqueous solution and silicon ethoxide [33].

2.1.2. Rapid route

The alkoxide mixture was diluted in propanol. A large excess of water (typical isopropanol/alkoxide/water volume ratios about 1/1.5/2), was used to achieve complete hydrolysis under vigorous mixing. Prior to hydrolysis, the alkoxide solution was heated for $\sim$ 1 h at 80° C. A typical batch used 50 cm^3 alkoxide. Gel powder was obtained after room temperature removal of the solvents (water and alcohols) under a moderate mixing. The powder was then dried between 30 and 50° C for one week and compacted as described previously [5]. Note that before recording Raman spectra, it was necessary to dry the sample for a few weeks at room temperature in a clean atmosphere in order to minimize fluorescence. This fluorescence could also be strongly decreased by exposing the sample for 1 h to the laser focus before recording the spectrum.

2.2. Characterization

The density of gels and thermally treated samples (monolithic pieces) was measured using the usual mass and volume determination. Various liquids can be used to measure the volume: water, alcohols, or DMSO; the measured volume must be a function of the penetration into the pores due to their various polar and protic characters. Apparent density can also be measured on pellets made by grinding and compaction (200 kN for

a pellet of 10 mm diameter) of gel. In the case of powdered materials, picnometry can also be used. Compositions were checked by chemical analysis.

Thermogravimetry (TG) was performed between 30 and 600° C and differential thermal analysis (DTA) between 30 and 1500° C using Dupont de Nemours Instruments. Differential scanning calorimetry (DSC) was recorded between 0 and 500° C under a nitrogen flux using a DSC4 Perkin–Elmer Instrument. Weight losses were measured after each run. X-ray powder patterns were recorded using $\lambda CuK\alpha$ radiation. Infrared spectra were obtained with a 783 Perkin–Elmer spectrophotometer using paraffin oil or Fluorolube mulls between CsI, CaF_2 or KRS5 windows.

Micro-probe Raman spectra were recorded with an Instrument S.A. Mole apparatus using a 1.5 W argon ion laser of Spectra Physics. The 514.5 nm excitation line was preferentially used in order to shift the fluorescence. Note that the ISA Mole Microprobe illuminates the sample and collects the Raman scattering through a microscope (magnification $\times 1000$). Thus the area examined is about a few square micrometres and it is possible to analyse many places at the surface or inside the optically clear samples. The large collection angle of the microscope allows the recording of spectra, even in the case of very poor scatterers, without local degradation due to a too high laser power. The power used at the sample ranged between 1 and 50 mW. The frequency accuracy was limited to $\pm 5\,cm^{-1}$.

3. Results and discussion

3.1. Evidence for distinct kinds of mullite gels

Gels may exhibit very different aspects and shapes. Gels prepared by slow hydrolysis in hexane are hard and optically clear. Gels made in propanol are often only transluscent at the surface. On the other hand, gels made with aluminium nitrate look soft, even a long time after gelation and drying.

Fig. 2 compares DSC traces of monoliths and powders. Except for the monoliths prepared with $Al(NO_3)_3$ aqueous solution and Si-ethoxide according to Yoldas [33], all DSC traces consist of one broad intense peak beginning at low temperature (50 to 80° C, in fact the drying temperature). In some cases a small peak occurs at about 300° C. Fig. 3 shows typical TGA traces. Weight losses of monoliths lie between $\simeq 33\%$ and 42% if the synthesis is made in hexane. This corresponds to the general formula $3Al_2O_3 \cdot 2SiO_2 \cdot 12$ to $14H_2O$. Gels prepared in propanol reach higher weight losses (40 to 50%). The corresponding formula is $3Al_2O_3 \cdot 2SiO_2 \cdot 25$ to $30H_2O$. As in the case of alumina gels, the weight loss is regular up to 250° C and a residual loss ($\sim 2\%$) occurs between 550 and 600° C. Sometimes a step is observed at 250 to 300° C in correlation with the presence of a second

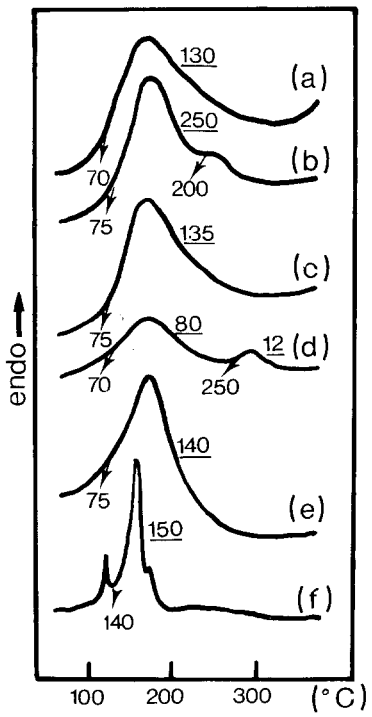

Figure 2 DSC traces of monoliths synthesized in hexane (a, d, e), in propanol (b, c) or using an aluminium nitrate solution [33] (f). Silicon methoxide (a, b), silicon ethoxide (c, d, f) and silicon propoxide (e) are used, respectively. (Heating rate $10°\,C\,min^{-1}$; enthalpies in $cal\,g^{-1}$.)

TABLE I Synthesis of mullite gels

Silicon alkoxide	Solvent (ratio)*	Hydrolysis medium	Gelation time	Drying time	Weight loss (%)	Density†	Remarks
Methoxide Dyna Ethoxide Dyna Butoxide Dyna Propoxide Dyna	Propanol‡ (1/1.5/2)	Water	inst.	1 w (40°)	40 ↓ 45	1.9–2.1	Powders Boehmite traces Boehmite and bayerite traces
Methoxide Dyna Ethoxide Dyna Butoxide Dyna Propoxide Dyna Ethoxide Alfa	Propanol (4/1)	Atmospheric moisture	1 to 4 w	4 w to 2 mon	45 ↓ 50 60–70	1.7–2	Optically clear monoliths 0.1–1 cm^3
Methoxide Dyna Ethoxide Dyna Butoxide Dyna Propoxide Dyna	Hexane or cyclohexane (4/1)	Atmospheric moisture	1 to 4 w	4 w to 2 mon	35 ↓ 40	1.7–2	Optically clear monoliths 0.1–1 cm^3

*Solvent/alkoxide/(water) ratio by volume.
†Compacted pellets ($g\,cm^{-3}$).
‡The aluminium butoxide is diluted four times in propanol before mixing with silicon alkoxide and solvent.
w: weeks.
mon: months.
inst: instantaneous.

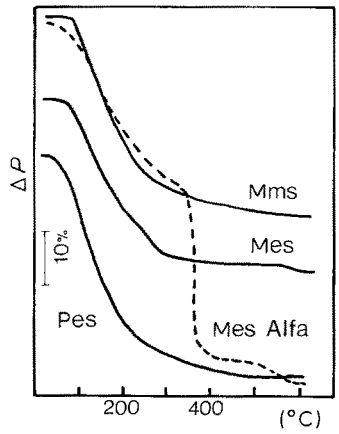

Figure 3 TGA traces of monoliths prepared in hexane (M) and powders (P) synthesized using silicon methoxide (ms) or silicon ethoxide (es). (Heating rate 100° C h^{-1}.)

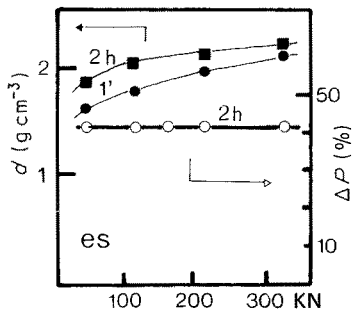

Figure 4 Evolution of the apparent density of compacted pellets and of the weight loss between 30 and 600° C as a function of the applied pressure and the duration. (Dynamit-Nobel silicon ethoxide is used.)

DSC peak. Note that the nature of the raw materials plays a prominant part: for instance, use of Alfa-Ventron silicon ethoxide leads to higher weight loss (60 to 70%): a marked jump is observed at about 240° C on the TGA trace (Fig. 3). A previous study [34] has shown that this alkoxide is quickly partially self-polymerized, due to the presence of trisilisic ester.

This partial polymerization might favour heterogeneity and thus the formation of aluminium hydrate. However, the gels are X-ray amorphous and no traces of $Al(OH)_3$ are visible on either infrared (IR) or Raman spectra.

The hydrolysis of mullite composition is more regular than that of pure alumina [14] and thus monoliths are more easily obtained in a shorter time.

Gel density ranges between 1.3 and 2.1 as a function of the solvent used for volume determination: the highest densities (1.7 to 2.1) are measured with DMSO, as this solvent penetrates the pores by removing water. The densities measured on compacted pellets vary between 1.9 and 2.1. Fig. 4 shows the evolution of the apparent density of pellets as a function of the applied pressure and for various pressing times. Note that the weight loss is not affected (in fact a small quantity of solvent is evacuated at the beginning of the compaction [5]). This densification involves a sintering phenomenon as previously observed for other gel compositions [5] and for hydrates [35]. In the case of powders, whatever the synthesis method, the apparent density of pellets is comprised between 2 and 2.1. Densities equal to 2 are also obtained using picnometry determination. All the values measured reach the 2.1 limit which can be considered as a realistic value which takes into account only the larger pores. By comparison with spinel ($\simeq 3.6$) and mullite ($\simeq 3.26$) densities, it is possible to evaluate the high number of network defects. The resulting porosity thus comprises between approximately 30% and 60%. Pore size (3 to 8 nm) of some mullite and alumina gels was previously determined by Yoldas [25] and Chane-Ching and Klein [36]. The corresponding porosity agrees with our results. This very large porosity explains the high quantity of water soaked in the pores.

Fig. 5 compares X-ray powder patterns of ground monoliths and of powders prepared by various methods. Patterns of monoliths are typical of amorphous structure, but the interreticular d-value of the first intense bump varies between 0.34 and 0.44 nm. This indicates various kinds of local structure. Note also that the small-angle scattering is variable. Powder patterns show boehmite-like peaks, their broadness decreasing with the increasing alkoxide length but remaining

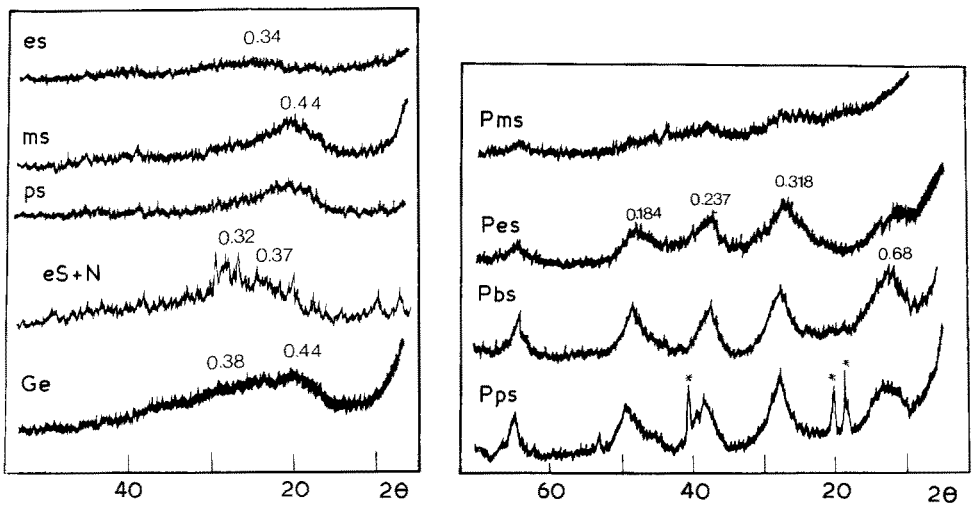

Figure 5 X-ray powder patterns (λCu$K\alpha$) of mullite monoliths prepared by slow hydrolysis in hexane and of powders (P) synthesized using the rapid hydrolysis route in propanol. Various silicon alkoxides have been used (ms, methoxide; es, ethoxide; bs, butoxide; ps, propoxide). Comparison with samples made from $Al(NO_3)_3$ aqueous solution and silicon ethoxide (es + N) mixture and with $AlGe_2O_7$ monoliths (germanium ethoxide being used) is also given. (*) $Al(OH)_3$ phase.

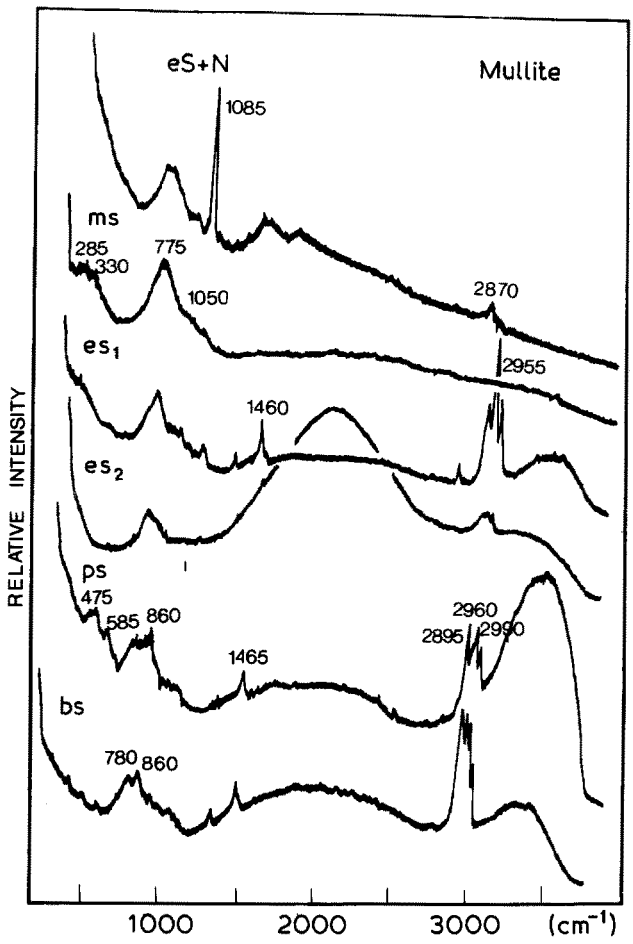

Figure 6 Micro-Raman spectra of optically clear monolithic gels prepared by various methods: hydrolysis of silicon ethoxide with an aqueous aluminium nitrate solution (es + N), of aluminium sec-butoxide and silicon methoxide (ms), silicon ethoxide (es1), silicon propoxide (ps) and silicon butoxide (bs) in hexane or in propanol (silicon ethoxide, es2).

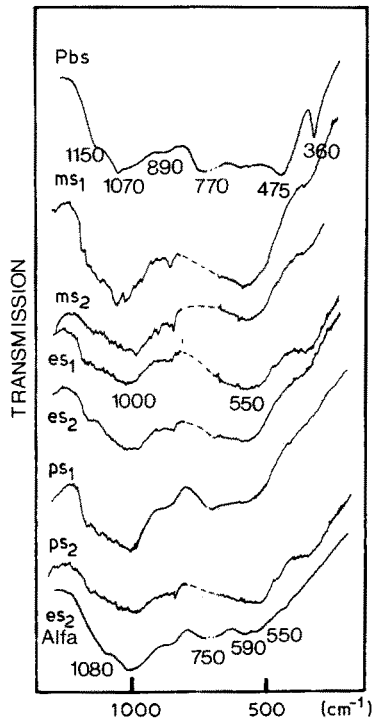

Figure 7 IR spectra of gels synthesized in hexane (ms1, es1, ps1) or in propanol (ms2, es2, es2-Alfa, ps2) using silicon methoxide (ms), silicon ethoxide (es) and silicon propoxide (ps). Pbs: powder prepared by the rapid hydrolysis route (with silicon butoxide).

larger than usually observed in true boehmite. If silicon propoxide is used, $Al(OH)_3$ traces are also observed. Note that the small-angle diffuse scattering decreases with the increase of crystalline traces.

Figs 6 and 7 show typical Raman and IR spectra of mullite monoliths and powders. Raman spectra show clearly that organic traces remaining in the gels (alcohols) increase from methoxide to butoxide (δCH_3 and νCH_3 modes occur at 1460 and 2900 to 3000 cm^{-1}, respectively). The Al–O and Si–O stretching and bending massifs (200 to 600 and 600 to 1200 cm^{-1}, respectively) are also different. By comparison with alumina gel spectra [14, 36] the intensities of the δO–H bands are weaker.

The very large bumps (Fig. 6) are related to the fluorescence phenomenon (they are more intense and appropriately shifted with the use of the 488 nm excitation line) but the presence of a νOH contribution in the 3000 to 3700 cm^{-1} range is not excluded.

3.2. Structure of gels

The Al_2SiO_5 polymorphs are commonly classed mineralogically as orthosilicates with isolated SiO_4 units embedded in an aluminate matrix. The highest frequency modes of these structures are derived from stretching internal vibrations. In order to apply this description to mullite polymorphs, we must assume that the tetrahedron-framework description is correct. Such an assumption was made previously by McMillan and Piriou [15] and Ishii *et al.* [9].

IR spectra of mullite gels are very similar to those of pure alumina gel [14], alumina glassy phase [14] and transition alumina phases [37], except for the lower intensity of the 800 to 1300 cm^{-1} region due to the absence of Si–O bonds. In the case of monoliths prepared from silicon methoxide and silicon ethoxide hydrolysis, the Raman spectra also resemble that of alumina. On the other hand, monoliths prepared with silicon propoxide and silicon butoxide show a more complex pattern with intense bands at 475 and 585 cm^{-1}. Such bands must be assigned to the presence of silica segregation (crystobalite traces are indeed observed in such samples after heating), the most intense bands in such compounds being the 425 cm^{-1} band (Fig. 6). Substitution of silicon by germanium (Fig. 8) leads to more structured spectra, with bands at lower frequency according to the mass effect ($\sqrt{Ge/Si} = 1.6$). "Germanium–mullite" glass shows Raman bands between 500 and 600 cm^{-1} as observed on the amorphous GeO_2 Raman spectrum (Fig. 8): they can be assigned to bridged tetrahedra (Ge–O–Ge stretching mode). It must be underlined that the preparation of amorphous GeO_2 is difficult. This is consistent with the more ordered spectra, although the X-ray powder pattern is very broad (Fig. 5).

Thus, the mullite gel seems to have the same structure as the alumina gel, i.e. a spinel-like structure made of AlO_4 and SiO_4 tetrahedra. In the case of optically clear monoliths, hydrate traces (AlOOH, $Al(OH)_3$) are never observed, in contrast to the case of pure alumina gel [14]. The presence of SiO_4 tetrahedra induces a more intense 950 to 1050 cm^{-1} Raman bump and the AlO_4 bending bands are well observed. This

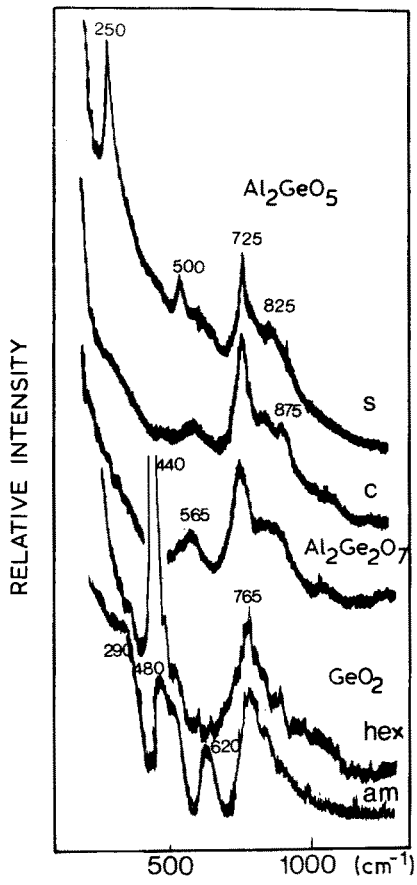

Figure 8 Micro-Raman spectra of Al_2GeO_5 (S, surface; C, core) and of Al_2GeO_7 monolithic optically clear gels. In comparison, spectra of alkoxide-derived amorphous (am, prepared according to [43]) and hexagonal (hex) GeO_2 powder are given.

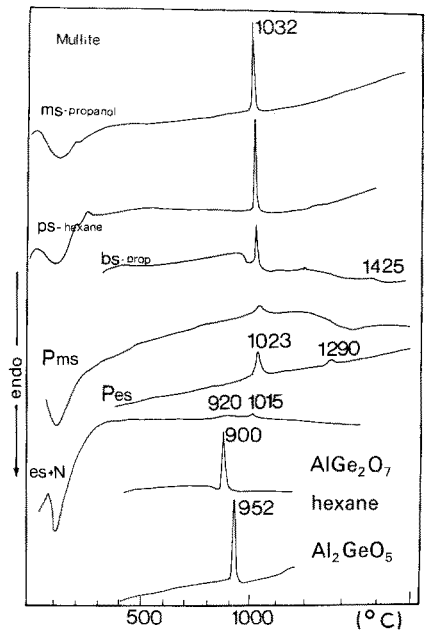

Figure 9 DTA traces of mullites, Al_2GeO_7 and Al_2GeO_5 monoliths synthesized in hexane and in propanol using silicon methoxide (ms), silicon propoxide (ps) and silicon butoxide (bs). Comparison is made with powder prepared with silicon methoxide (Pms) or silicon ethoxide (Pes) and with monoliths prepared with aluminium nitrate solution (es + N). (Heating rate 20° C min^{-1}.)

indicates that the presence of silicon alkoxide regularizes the aluminium butoxide hydrolysis and favours the homogeneity. On the other hand, in the case of powder synthesized through the rapid route, the vibrational spectra confirm the X-ray analysis. The 360 cm^{-1} IR band is characteristic of boehmite. Bayerite traces can be observed if silicon-propoxide is used (Fig. 5). If a nitrate solution is used, the corresponding intense stretching mode is observed (e.g. at 1085 cm^{-1} on the Raman spectrum).

3.3. Glass formation and crystallization

Fig. 9 shows DTA traces of typical mullite monoliths and powders. An intense exothermic peak is observed between 1020 and 1030° C and sometimes a second, weaker one, is observed between 1230 and 1425° C. In the case of nitrate gels, another peak is observed at 920° C before the small 1015° C peak. Peaks are observed at lower temperature for germanium homologues, e.g. at 900 and 952° C for Al_2GeO_7 and Al_2GeO_5, respectively. Peak intensities are lower for powders produced by rapid hydrolysis with excess water than those observed for monoliths. Note that in some cases a "glass transition" anomaly is observed just before the intense exotherm.

X-ray powder patterns remain typical of amorphous materials up to 900° C and then a progressive transformation into "γ-alumina-like" pattern is observed and the pores close. This transformation is more visible for samples synthesized from silicon propoxide and silicon butoxide (Fig. 10). Above the exothermic peak the mullite phase is observed, but the crystallinity (peak intensity modification, narrowing) increases regularly with the temperature and not with the duration of annealing (hours, days or weeks). Note that a bump still remains at $d = 0.4$ nm for 1100° C heated ($x = 0.25$) mullite. Monoliths remain optically clear up to 1480° C in the case of hexane synthesis using silicon methoxide or silicon ethoxide and up to 1300° C for all syntheses in hexane or propanol. The second exotherm can sometimes be correlated with the formation of crystobalite traces (for instance for some powder preparations), but in many cases no such traces are detected. We also note that the splitting of the 3.42 to 3.38 nm Bragg peaks can be well observed soon after a 1300° C heating for aluminium-rich compositions.

Fig. 11 compares the corresponding Raman spectra. Up to the exothermic peak, the Raman spectra of $x = 0.25$ mullite remain similar to that of the gel, except for the disappearance of the bands due to organic traces and protonic species bands (Table II). With the formation of crystalline mullite we observe new bands at 320, 430 and 970 cm^{-1} (frequency accuracy $\sim \pm 10\,cm^{-1}$). The degree of modification depends upon the synthesis method. Band narrowing is observed up to 1500° C.

The fact that monoliths remain optically clear and that the evolution of the spectra is progressive indicates that the transformation gel → glass → spinel → mullite is "continuous". Comparison of Raman spectra (Fig. 11) of 1400° C annealed samples having various compositions between $x = 0$ and $x = 0.5$ shows the same picture as the comparison of $x = 0.25$ samples sintered between 1000 and 1500° C (Fig. 12). However the X-ray powder patterns are different and well-

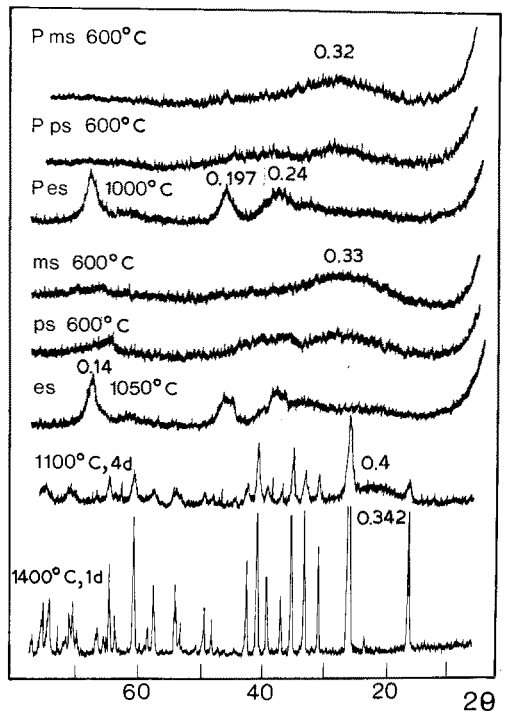

Figure 10 X-ray powder patterns ($\lambda CuK\alpha$) of mullite glass and ceramics issued from powders (rapid hydrolysis in propanol, P) and of monoliths (slow hydrolysis in hexane) and heated 2 h at 600, 1000 or 1050° C, 4 d at 1100° C and 1 d at 1400° C, respectively. Silicon methoxide (ms), silicon ethoxide (es) and silicon propoxide (ps) have been used (d in nm).

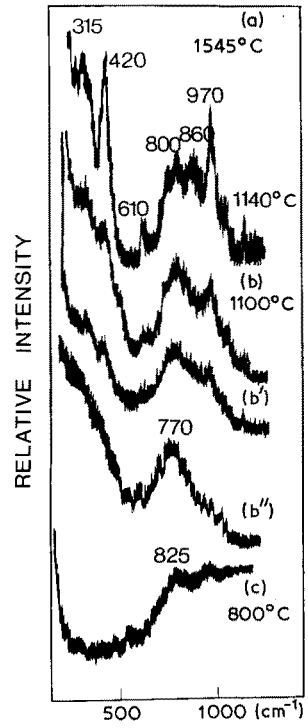

Figure 11 Micro-Raman spectra of mullite ($x = 0.25$) optically clear samples produced from slow hydrolysis in hexane using silicon propoxide (a), silicon methoxide (b'), silicon ethoxide (b'', c) and heated 4 d at various temperatures. For comparison, the spectrum of a monolith prepared using $Al(NO_3)_3$ solution is also given (b).

crystallized mullite is only observed above 1300° C. Sillimanite composition ($x = 0$) shows the most ordered spectra, which can indicate an ordering but on a more local scale than in natural true sillimanite [11].

3.4. Assignment of the spectra

Before discussing the assignment of our spectra, we will recall the main results concerning the parent compounds (Table II).

Stretching SiO_4 modes are observed between 850 and 1150 cm^{-1}, the strongest Raman high-frequency modes being at 715, 877, 955 and 921 cm^{-1} for shiastovite, sillimanite, kyanite and andalousite, respectively [9, 11, 15, 38, 39]. The mullite spectra of McMillan and Piriou [15] show an intense band at 960 cm^{-1}. This frequency is then similar to those of NASICON (an acronym for the Na Super Ionic Conductor, $Na_{1+x}Zr_2Si_xP_{3-x}O_{12}$); in this structure the tetrahedra are also isolated [6]. The vibrational calculation for andalousite [9] did not find vibrations involving pure Al–O internal modes, except for a Raman band near 700 cm^{-1} and its infrared counterpart at 620 to 675 cm^{-1}. The 798 cm^{-1} Raman bands may also have a large component of Al–O stretching. This is consistent with our assignment concerning alumina gels and glasses having a spinel-like structure [14, 32] and with the assignment of the spectrum of $MgAl_2O_4$ (Fig. 13 [40]). The comparison of mullite and kyanite spectra shows clearly the narrowing due to the disappearance of the Al/Si substitution disorder, only SiO_4 tetrahedra being present in kyanite. Thus the 980 and 780 cm^{-1} bands can be assigned to Si–O and Al–O (ν_3) stretching modes and the 410 and 300 cm^{-1} bands to the Si–O and Al–O (ν_2) bending modes. The 600 to 700 cm^{-1} massif can be assigned to the other ν_4 bending mode (Table II).

Raman spectra of mullite are very dependent on the history of the samples. Fig. 13 compares spectra from McMillan and Piriou [15] with those of a mullite single crystal and with the spectrum of an SiO_2–mullite composite prepared from rapid cooling from the melt [41, 42]. We observe that the broadness of the bands is different as a function of the samples and as a function of the bands. For instance the ν_2 bending Si–O mode at 410 cm^{-1} has a full-width at half-height (FWHH) of $\simeq 50$ cm^{-1} whereas the FWHH of the Al–O mode is larger than 200 cm^{-1} (Fig. 12). This phenomenon is also observed for metakaolinite, SiO_2–crystobalite [14] and GeO_2-quartz (Fig. 8) and for kyanite (Fig. 13). Such differences have also been observed in NASICON and are assigned to the large orientational disorder of the tetrahedra in the structure [6]. Band intensity changes are also observed. (The grain size of the samples being lower than 1 μm, the micro Raman spectra of present ceramics can be considered as powder spectra.) The differences are thus related to structural modifications and the narrowing of the 970 cm^{-1} band can be assigned to the ordering of SiO_4 tetrahedra.

The nature of the spinel intermediate phase (pure alumina, spinel with mullite composition, spinel with $6Al_2O_3 \cdot 1SiO_2$ composition, etc.) and the presence of amorphous silica have been questioned as reported in Section 1. X-ray powder patterns (Fig. 10) can show a bump at 0.4 nm, which must correspond to amorphous SiO_2 or to the remaining amorphous mullite. In our vibrational spectra, there is no evidence of such amorphous silica, but this is not proof, spinel and alumina being poor Raman scatterers, the

TABLE II IR and Raman frequencies of mullite and parent compounds

Assignments	Sillimanite [15, 38]		Andalousite [9, 38, 39]		Mullite [15, 18]		Needle (this work) R	Eutectite (this work)		Mullite glass (this work)		Mullite with spinel structure (this work)		Mullite gel (this work)	
	IR	R	IR	R	IR	R		IR	R	IR	R	IR	R	IR	R
	1195 sh											1220 sh			
	1175 s			1100 w	1175 s	1160 m		1155 m	1140 m	1170 s		1160 sh			
$\nu_3 SiO_4$		1131 w	1005 sh		1120 m		1125 w	1110 sh			1100 m	1085 s		1080 m	1050 sh
			970 m		1000 m	1040 sh	1050 w		1030 m	1050 s			1000 sh	1000 s	
	955 m		940 s	950 s	960 m	960 s	960 s	960 sh	970 s		980 w				900 sh
	910 s	906 s			927 s			930 s						890 m	
					901 s										
$\nu_1 SiO_4$	882 m	873 s	895 m												
	815 s			850 w		880 m									
		789 w	774 w		832 s		780 m	840 s	780 s	840 s	820 s	840 m	770 s		790 ± 20 s
	745 m	711 m	737 w		740 m										
T'O–Al (oct)	690 s	702 m	688 s	700 m	725 w	710 m								750 m	
	630 w		609 s		640 w	610 m			620 s			680 m			
(T'O–Al)	582 s	597 m			613 m		600 w			640 sh			600 w		
(tetra)	540 sh	534 m			567 s			565 s							
							550 w			550 sh		560 m		550 s	
$\nu_4 SiO_4$	525 sh		520 m		542 s										
	502 s			500 m	500 s										
	490 sh		480 w												
$\nu_2 SiO_4$	437 s		450 s		445 m			450 sh							
		422 w			420 w	410 s	410 s	430 sh	420 s	455 m	450 w	470 m	400 w		
T'Al	370 m	392 w	390 w												
R', $T'SiO_4$	342 w		358 w	350 s	362 w										
	330 m				344 w										
	320 w	310 m	303 s		306 w	3105	320 w		310 s		350 sh	350 w			330 ± 20 sh
T'Al–O	262 s							260 w	240 sh						
		236 m													
	202 s		204 w	200 m			220 m								250 ± 30 m
		142 m			*	150 m		*	*	*	*	*	*	*	
T'Al, SiO_4	115 w														
		99 w		100 w											
		70 w													

s, strong; m, medium: w, weak; sh, shoulder.

*IR spectra below 250 cm^{-1} have not been recorded.

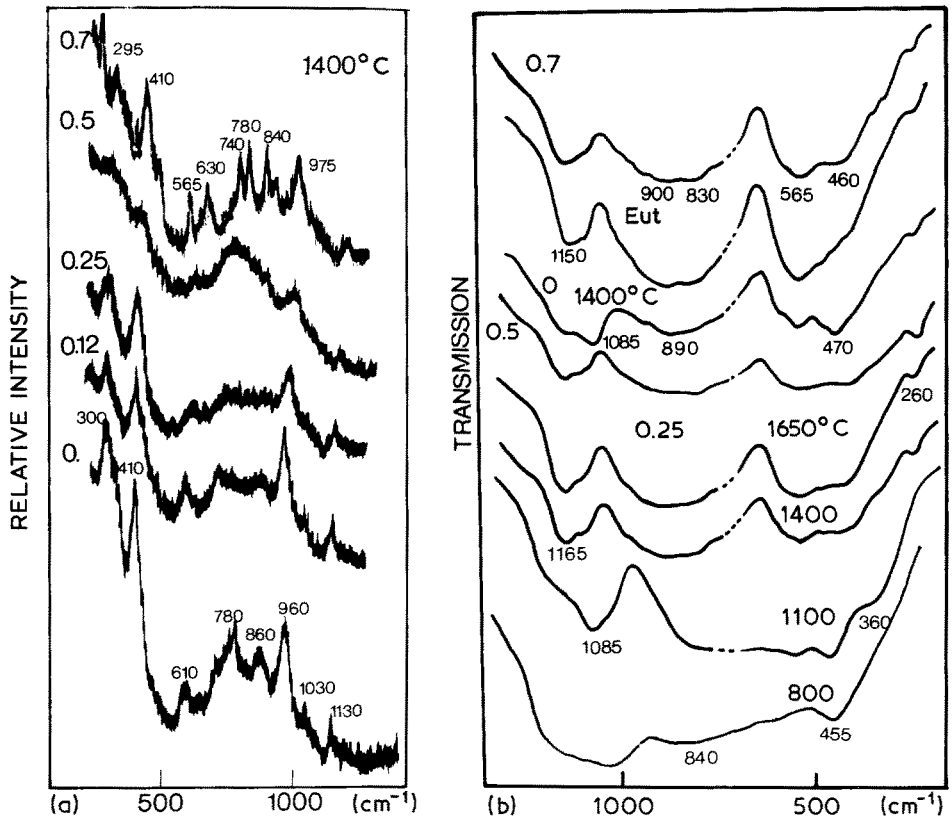

Figure 12 Micro-Raman (a) and IR (b) spectra of mullite monoliths of various compositions ($0 \leqslant x \leqslant 0.7$) prepared by slow hydrolysis of aluminium butoxide and silicon methoxide in hexane and heated for 1 w at various temperatures between 800 and 1650° C. Monoliths with compositions $x = 0.5$; 0.25 and 0.12 are optically clear. IR spectrum of silica–mullite composite [42] is also given (Eut).

silica spectra might be observed. On the other hand, the preservation of the optical clarity of the monoliths up to 1500 to 1600° C indicates that only one phase is present, at last at the 0.1 μm scale. Thus, our opinion is that no segregation takes place during the transformation gel → orthorhombic mullite. A progressive ordering at local scale takes place. The X-ray powder patterns and the DTA traces indicate a strong modification in the 1000 to 1100° C temperature range. The decrease of the orientational disorder can explain the narrowing of the SiO_4 (above 1000° C) and AlO_4 (above 1300° C) stretching modes. The other counterparts on Raman spectra are the condensation of the bending modes below 500 cm^{-1}, the frequency shift of the Al–O "stretching mode" (from 820 to 770 cm^{-1}) indicating a considerable strengthening of the bond at the glass → spinel transition. The mean Al–O frequency increases when the mullite phase occurs according to the unit cell dilatation. (The recording of the low-frequency spectra is not possible with our apparatus.) As far as the IR spectra are concerned, the narrowing of the bands is clearly visible on Fig. 12. The spinel-like phase is characterized by the 350 cm^{-1} shoulder and the appearance of the 550 cm^{-1} band. The shift of the mean Si–O and Al–O stretching modes is straightforward.

The comparison of the IR and Raman spectra of various samples heated at 1400° C (Fig. 12) shows

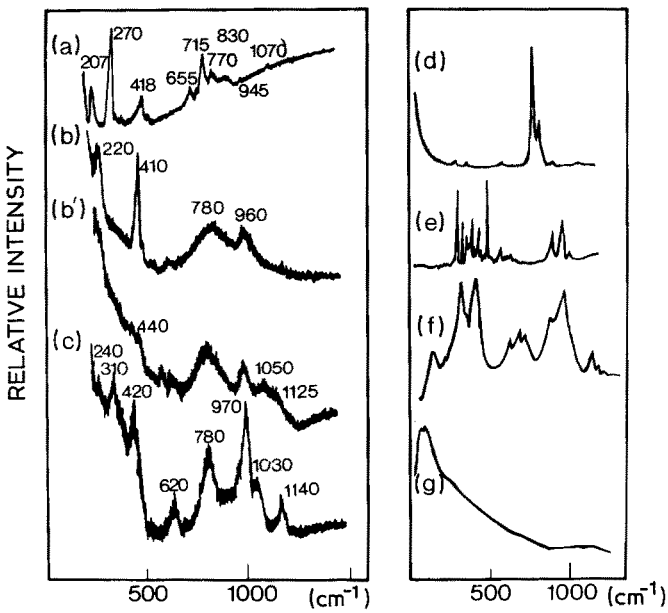

Figure 13 Raman spectra of (a) natural shiastovite of Ruanda (sillimanite-type); (b) mullite single crystal on the needle or (b') on the front, with composition close to $x = 0.4$ [41]; (c) SiO_2–mullite composite with composition close to $x = 0.2$ [41], (d) Mg_2SiO_4 [40], (e) kyanite; (f) mullite from [15], and (g) 0.59 Al_2O_3–0.41SiO_2 glass [15].

clearly that sillimanite composition has a narrower spectrum. We also observe that Al–O modes broaden very rapidly with aluminium addition and this phenomenon is easily understood if we observe the structure modification given in Fig. 1. On the other hand aluminium-rich compositions (above the usual limits of the mullite solid solution) show a spectrum with narrow bands superimposed on the broad feature of the $x = 0.5$ composition. This does not seem to be related to a precipitation of corundum, but rather to the presence of two kinds of local environment as proposed by Angel and Prewitt [10].

The narrower Raman spectra are observed for the SiO_2–mullite composite (Fig. 12) and the broader ones for the single crystal (Fig. 13) as far as the stretching modes are concerned. The compositions of these materials are close to $x = 0.2$ and 0.4, respectively [41, 42]. Ceramics produced from sol–gel preparation show intermediate behaviour. Note also that the broadness is different as a function of the modes: even in the crystal, the bending mode is considerably narrower than the stretching mode, which can be the indication of a great orientational disorder.

4. Conclusion

The local structure of optically clear monolithic gels has been interpreted on the basis of vibrational spectroscopy as a spinel-like structure.

The formation of orthorhombic mullite appears rather progressive. The local structure is little modified upon formation of the glassy state and mullite is formed in the 1000 to 1100° C temperature range through an intermediate spinel "structure". The local structure evolution is not so drastic as it can be deduced from DTA or X-ray analysis. The evolution is observed up to 1600° C but the monoliths remain optically clear. The non-stoichiometry and the synthesis method modify the local structure. The ordering is consistent with both local Si/Al position ordering above the first intense exotherm and with a progressive decrease of the orientational disorder of the tetrahedra in the 1050 to 1400° C temperature range.

Acknowledgements

Dr D. Michel and L. Mazerolles are thanked for the gift of mullite single crystal and composite samples and for helpful discussions. The author also thanks Dr D. W. C. Smith for communication of data on natural mullites.

References

1. S. SAKKA and K. KAMIYA, *J. Non-Crystalline Solids* **42** (1980) 403.
2. D. W. JOHNSON Jr, *Amer. Ceram. Soc. Bull.* **64** (1985) 1587.
3. L. L. HENCH and D. R. ULRICH (eds), "Ultrastructure Processing of Ceramics, Glasses and Composites" (Wiley, New York, 1984).
4. K. S. MAZDIYASNI, *Ceram. Int.* **8** (1982) 42.
5. Ph. COLOMBAN, *Ceramics Int.* **15** (1989) 23.
6. Ph. COLOMBAN, *Solid State Ionics* **21** (1986) 97.
7. C. N. BURNHAM, *Carnegie Inst. Year Bk* **63** (1963) 223.
8. J. YLA-JAASHI and H. U. NISSEN, *Phys. Chem. Minerals* **10** (1983) 47.
9. K. IISHII, E. SALJE and Ch. WERNEKE, *ibid.* **4** (1979) 173.
10. R. J. ANGEL and C. T. PREWITT, *Acta Crystallogr.* **B43** (1987) 116.
11. E. SALJE and Chr. WERNEKE, *Contr. Minerals Petrol.* **79** (1982) 56.
12. D. G. W. SMITH and J. D. C. McCONNELL, *Min. Mag.* **35** (1964) 811.
13. J. K. WINTER and S. GHOSE, *Amer. Mineral.* **69** (1979) 573.
14. Ph. COLOMBAN, *J. Mater. Sci.* **24** (1989) 3002.
15. P. McMILLAN and B. PIRIOU, *J. Non-Cryst. Solids* **53** (1982) 279.
16. M. TOKONAMI, Y. NAKAJINA and N. MORIMOTO, *Acta Crystallogr.* **A36** (1980) 270.
17. K. S. MAZDIYASNI and L. M. BROWN, *J. Amer. Ceram. Soc.* **55** (1972) 548.
18. H. J. PERCIVAL, J. F. DUNCAN and P. K. FOSTER, *ibid.* **57** (1974) 57.
19. A. K. CHAKRABORTY and D. K. GHOSH, *ibid.* **61** (1978) 170.
20. M. BULENS, A. LEONARD and B. DELMON, *ibid.* **61** (1978) 81.
21. S. PROCHAZKA and F. J. KLUG, *ibid.* **66** (1983) 874.
22. D. W. HOFFMAN, R. ROY and S. KOMARNENI, *ibid.* **67** (1984) 468.
23. J. A. PASK, "Current Understanding of Stable and Metastable Phase Equilibria and Reactions in the SiO_2–αAl_2O_3 System", in "Ceramic Powders", edited by P. Vincenzini, Materials Science Monograph 16 (Elsevier, Amsterdam, 1983) pp. 21–32.
24. A. K. CHAKRAVORTY and D. K. GHOSH, *J. Amer. Ceram. Soc.* **69** (1986) C202.
25. B. F. YOLDAS, *Amer. Ceram. Soc. Bull.* **59** (1980) 479.
26. K. OKADA, N. OTSUKA and J. OSAKA, *J. Amer. Ceram. Soc.* **69** (1968) C251.
27. S. KANZAKI, H. TABATA, S. KUMAZAWA and S. OHTA, *ibid.* **68** (1985) C6.
28. Y. SUWA, R. ROY and S. KOMARNENI, *Mater. Sci. Engng* **83** (1986) 151.
29. Y. M. M. AL-JARSHA, K. D. BIDDLE, A. K. DAS, T. J. DAVIES, H. G. EMBLEM, K. JONES, J. M. McCULLOUGH, M. A. MOHD ADD. RAHMAN, A. N. A El-M. SHARF EL DEEN and R. WAKEFIELD, *J. Mater. Sci.* **20** (1985) 1773.
30. M. OHASHI, H. TAKOTA, O. ABE, S. KANZAKI, S. MITACHI and T. KUMAZAWA, *J. Mater. Sci. Lett.* **6** (1987) 528.
31. K. OKADA and N. OTSUKA, *J. Amer. Ceram. Soc.* **69** (1986) 652.
32. Ph. COLOMBAN, "Structure of Alumina, Mullite and Zirconia Gels and Glasses using Raman Microprobe", Proceedings of the 11th International Conference on Raman Scattering, London, 5th to 9th September, edited by J. F. Gibson (Wiley, London, 1988) p. 507.
33. B. E. YOLDAS, *Amer. Ceram. Soc. Bull.* **54** (1975) 289.
34. J. C. POUXVIEL, J. P. BOILOT, J. C. BELOEIL and J. Y. LALLEMAND, *J. Non-Cryst. Solids* **89** (1987) 345.
35. P. E. CHILDS, A. T. HOWE and M. G. SHILTON, *J. Solid State Chem.* **34** (1980) 341.
36. J. Y. CHANE-CHING and L. C. KLEIN, *J. Amer. Ceram. Soc.* **71** (1988) 86.
37. P. FORBES, J. DUBESSY and C. KOSZTOLANYI, *Terra Cognita* **7** (1987) 16.
38. S. W. KIEFFER, *Rev. Geophys. Space Phys.* **17** (1979) 20.
39. M. A. ALVAREZ and R. COY-YIL, *Anals de Quimica* **74** (1978) 1375.
40. P. McMILLAN and M. AKAOGI, *Amer. Mineral.* **72** (1987) 361.
41. L. MAZEROLLES, Thesis, University of Paris VI (1988).
42. L. MAZEROLLES, D. MICHEL and R. PORTIER, *Silicates Ind.* (1989) L111 (7-8) 97.
43. O. YAMAGUCHI and K. SHIMIZU, *Adv. Ceram.* **21** (1987) 163.

Received 28 April
and accepted 8 September 1988